Journal of Materials Chemistry C

ROYAL SOCIETY OF CHEMISTRY

PAPER

View Article Online
View Journal | View Issue

Cite this: J. Mater. Chem. C, 2022, 10, 4831

A solution-processable near-infrared thermally activated delayed fluorescent dye with a fused aromatic acceptor and aggregation induced emission behavior†

Daniel G. Congrave,‡*[a] Bluebell H. Drummond,‡[b] Qinying Gu,‡[b] Stephanie Montanaro,[c] Haydn Francis,[ad] Víctor Riesgo-González,[ad] Weixuan Zeng,[a] Campbell S. B. Matthews,[b] Simon Dowland,[b] Iain A. Wright,[c] Clare P. Grey,[a] Richard H. Friend[b] and Hugo Bronstein *[ab]

Received 5th October 2021,
Accepted 4th January 2022

DOI: 10.1039/d1tc04753a

rsc.li/materials-c

The unique synergy of properties offered by an efficient and processable near-infrared thermally activated delayed fluorescent (NIR TADF) dye could be transformative across research fields. Here, a solution-processable NIR TADF material is demonstrated (**CAT-TPE**). Good solubility is achieved through the use of a new tetraphenylethylene (TPE)-based triphenylamine electron donor. TADF is confirmed through variable temperature time-resolved measurements at a peak photoluminescence (PL) wavelength of 842 nm in a solution-processed film. An OLED with good roll-off characteristics for a solution-processed NIR TADF device is reported with electroluminescence $\lambda_{max} > 700$ nm. **CAT-TPE** also demonstrates classic aggregation induced emission (AIE) behavior, being more emissive when aggregated than in solution with all PL > 700 nm. This work opens the door to the considerably enhanced structural diversity of solution-processable NIR TADF and will inform the design of future high efficiency AIE NIR TADF materials.

Introduction

The near-infrared (NIR) region of the electromagnetic spectrum is broadly important across optoelectronic and biological applications.[1] NIR luminophores exhibiting thermally activated delayed fluorescence (TADF) are a particularly appealing class of material because they have the potential for a unique synergy of properties such as zero loss to triplet states, multicomponent luminescence lifetimes, and responsivity to external stimuli *e.g.* temperature, polarity and local oxygen content.[2–5]

A practical NIR TADF material must combine desirable electronic, optical and physical properties, particularly a low band-gap, small singlet–triplet exchange energy (ΔE_{ST}), low non-radiative loss[6–9] and good processability. By far the most common and well established strategy for the design of TADF dyes has been the connection of polycyclic aromatic electron donors (D) and acceptors (A) *via* twisted linkages.[10–12] For example, toward efficient NIR TADF,[13,14] specialized rigid (low non-radiative loss) electron acceptors have been developed that present both a low local triplet energy (small ΔE_{ST}) and a high electron affinity (narrow band-gap).[15–23] Such properties are usually achieved through adopting an extended fused π system with numerous electron withdrawing moieties *e.g.* nitriles, pyrazines and pyridines – structural components that are unfortunately also known to heavily restrict materials solubility.[24–26] For example, while offering NIR emission, our previously reported TADF material **CAT-1** suffers from poor solubility in organic solvents which precludes solution processing.[27] The processing of all champion fused aromatic NIR TADF dyes reported to-date is similarly restricted to thermal evaporation, to the best of our knowledge.[15–23,28] In fact, the availability of solution-processable NIR TADF materials is solely restricted to the boron curcuminoids introduced by Adachi *et al.*[29–31] Greater structural diversity in solution-processable materials is required if large area processing is to become a reality for NIR TADF.

Aggregation induced emission (AIE) is a phenomenon of great relevance to NIR TADF. Firstly, AIE offers an opportunity to take advantage of intermolecular rigidification to restrict molecular vibrations and add an extra dimension to reduce

[a] Yusuf Hamied Department of Chemistry, Lensfield Road, Cambridge, CB2 1EW, UK. E-mail: dc704@cam.ac.uk, hab60@cam.ac.uk
[b] Cavendish Laboratory, Cambridge, CB3 0HE, UK
[c] Department of Chemistry, Loughborough University, Loughborough, LE11 3TU, UK
[d] The Faraday Institution, Quad One, Harwell Science and Innovation Campus, Didcot, UK

† Electronic supplementary information (ESI) available. See DOI: 10.1039/d1tc04753a
‡ These authors contributed equally.

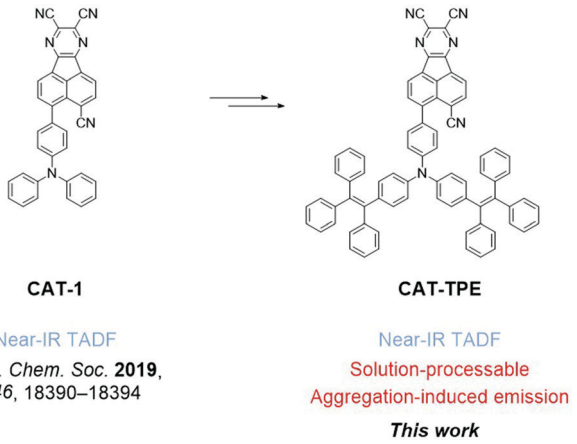

Fig. 1 Structure of CAT-TPE.

non-radiative decay in NIR materials.[20,29,32–38] Secondly, NIR AIE is promising in biological applications[39,40] which could benefit from the stimuli responsive behavior of TADF dyes.

In this work we devise a tetraphenylethylene (TPE)-fused triphenylamine (TPA) electron donor. The new donor can simultaneously endow good solubility and AIE behavior, culminating in the development of an AIE luminophore (**CAT-TPE**) which represents the first solution-processable NIR TADF material with a fused polycyclic aromatic electron acceptor (Fig. 1). **CAT-TPE** demonstrates the lowest energy TADF yet confirmed by variable temperature time resolved measurements. Additionally, solution-processed OLEDs are reported with λ_{max} beyond 700 nm.

Results and discussion

The novel TPE donor **4** was first synthesized according to a conventional route (Scheme 1). The TPE motif was selected because as well as being sufficiently bulky to suppress π–π stacking and enhance solubility, TPE-based luminophores often exhibit intense PL in the solid state.[41] We started from the brominated TPA **1**, which was subjected to Friedel–Crafts acylation to afford **2**. This route allows the use of an excess of benzoyl chloride to drive double acylation without the risk of triple acylation that would be encountered when starting with unsubstituted TPA.[42] Treatment with the diphenylmethane anion followed by dehydration with *para*-toluenesulfonic acid afforded the brominated donor **3**, which was converted to **4** *via* Miyaura borylation. As the TPE groups are incorporated into the TPA moiety rather than pendant, and both bromo (**3**) and boronic ester (**4**) functionalities are accessible, this new donor has great potential for generality in any donor–acceptor material. **CAT-TPE** was next prepared by sequential Suzuki coupling and condensation reactions. **CAT-TPE** is sufficiently soluble in common chlorinated and aromatic solvents (*e.g.* dichloromethane, chloroform, toluene and chlorobenzene) to be solution-processed. **CAT-TPE** demonstrates high decomposition (T_d = 514 °C) and glass transition (T_g = 173 °C) temperatures (Fig. S12, ESI†).

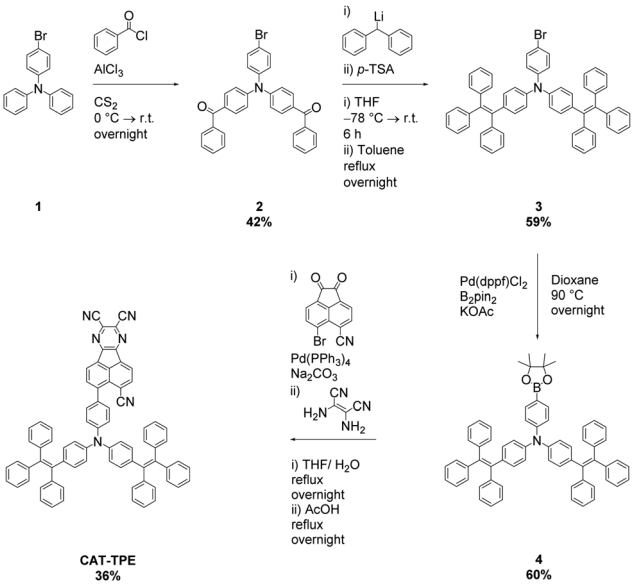

Scheme 1 Synthesis of CAT-TPE.

The absorption spectrum for **CAT-TPE** in dilute toluene solution is presented in Fig. 2 alongside that of **CAT-1** to illustrate the intrinsic effect of the TPE donor modification in the absence of aggregation. When the absorption spectra are normalized to the CT absorption band, the high energy transitions < 400 nm are clearly more intense for **CAT-TPE** than for **CAT-1**. This is rationally assigned to increased local π–π* transitions on the TPE donor, which possesses a larger number of phenyl groups than TPA. The CT absorption band for **CAT-TPE** (λ_{max} = 605 nm) is bathochromically shifted compared to that of **CAT-1** (λ_{max} = 560 nm). This is ascribed to the increased donor strength of our TPE donor compared to TPA, which is observed by cyclic voltammetry (Fig. 3 and Table 1) (**CAT-TPE** HOMO = −5.51 eV, **CAT-1** HOMO = −5.64 eV). As well as an electrochemically reversible reduction, we note that a reversible oxidation process is also observed for **CAT-TPE**, in contrast to **CAT-1**. The improved electrochemical stability of **CAT-TPE** is attributed to the bulky TPE groups, which prevent the dimerization of radical cations typically associated with TPA electron donors.[43]

The photoluminescence (PL) spectra and data recorded for drop-cast pristine and doped films of **CAT-TPE** are presented in Fig. 2 and Table 2, respectively. Only trace PL is detected for **CAT-TPE** in toluene solution, which is expected as TPE groups are well established to quench solution PL through intramolecular motion.[41] However, significant intramolecular charge-transfer (ICT) PL is observed when **CAT-TPE** is doped into a rigid TPBi matrix. Doped into TPBi at 5 wt%, **CAT-TPE** displays PL at λ_{max} = 752 nm with a photoluminescence quantum yield (PLQY, Φ_{PL}) of 11.3 ± 0.5% in the absence of oxygen. The PL is substantially quenched under air (Φ_{PL} = 7.4 ± 0.3%) (Fig. S2, ESI†). Delayed fluorescence with a lifetime (τ) of 16 μs also contributes to 6.6% of the integrated PL intensity (Fig. 2c). Variable temperature PL measurements indicate that

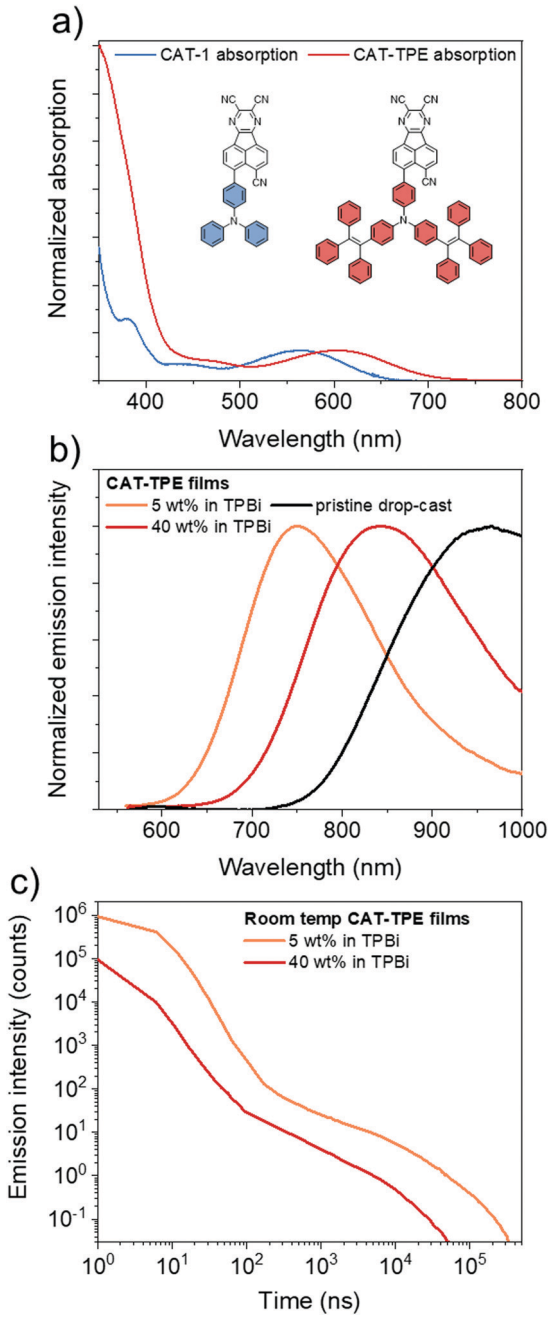

Fig. 2 (a) Absorption spectra of **CAT-1** and **CAT-TPE** in toluene solution; (b) photoluminescence spectra of **CAT-TPE** films (λ_{exc} = 405 nm); (c) integrated photoluminescence kinetics of **CAT-TPE** films under vacuum (λ_{exc} = 400 nm, 10^{-5} mbar).

the delayed component is thermally activated with an activation energy of 30 ± 5 meV (Fig. S4, ESI†), confirming the TADF behavior of **CAT-TPE**. TD-DFT predicts a ΔE_{ST} of 80 meV for **CAT-TPE** (Fig. S11 and Table S3, ESI†).

Increasing the concentration of **CAT-TPE** in TPBi red-shifts the PL λ_{max}, which we attribute to the combined effects of solvatochromism and aggregation. Hence, for **CAT-TPE** the TPE groups do not seem to completely suppress intermolecular interactions in the solid state. At 40 wt% in TPBi PL is recorded

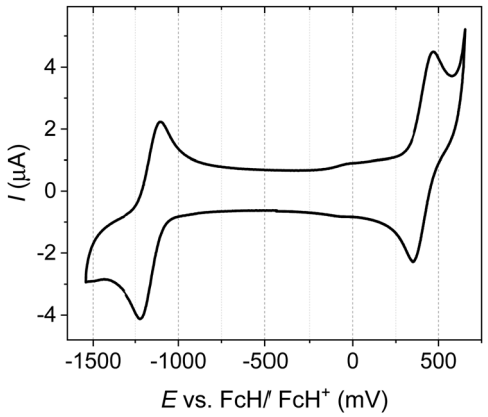

Fig. 3 Cyclic voltammogram recorded for **CAT-TPE** with 0.1 M n-Bu_4NPF_6 in THF as the supporting electrolyte (scan rate = 100 mV s^{-1}).

Table 1 Electrochemical data

E^{ox}/V $E_{pa}/E_{pc}[E_{1/2}]$	E^{red}/V $E_{pa}/E_{pc}[E_{1/2}]$	HOMO/eV[a]	LUMO/eV[a]	E_g[b]/eV
0.47/0.35 [0.41]	−1.10/−1.22 [−1.16]	−5.51	−3.94	1.57

[a] HOMO and LUMO levels calculated from CV potentials using the HOMO of ferrocene (−5.10 eV) as the standard, HOMO = −5.10 + $(-E_{1/2}^{ox})$ and LUMO = −5.10 + $(-E_{1/2}^{red})$. [b] Electrochemical HOMO–LUMO gap.

Table 2 Photophysical data

Sample preparation	λ_{max} PL/nm	PLQY[a]/%
5 wt% in TPBi	752	11.3 ± 0.5
10 wt% in TPBi	784	2.7 ± 0.1
40 wt% in TPBi	842	0.64 ± 0.03
Pristine drop-cast	961	<0.64

[a] Absolute PLQY measured using an integrating sphere.

with PL λ_{max} = 842 nm. This is accompanied by a decrease in Φ_{PL} to 0.64 ± 0.03%. Despite such a significant depression in Φ_{PL}, we note that when doped into TPBi at 40 wt%, **CAT-TPE** emits with a PL λ_{max} 60 nm redder than a neat film of the solution-processable boron curcuminoid reported by Adachi *et al.*[30] Furthermore, TADF behavior of the 40 wt% film is also confirmed; the PL has a lifetime of 4 μs (8.4% integrated contribution) and an activation energy of 19 ± 12 meV (Fig. S4, ESI†). Therefore, to the best of our knowledge, as well as clearly being the reddest solution processable TADF material, **CAT-TPE** displays the longest wavelength TADF yet confirmed by variable temperature PL measurements for any luminophore, solution-processed or evaporated. The PL of a pristine drop-cast film is impressively further red shifted close to 1 μm (PL λ_{max} = 961 nm), although the low PLQY complicates unambiguous confirmation of TADF under these sample preparation conditions.

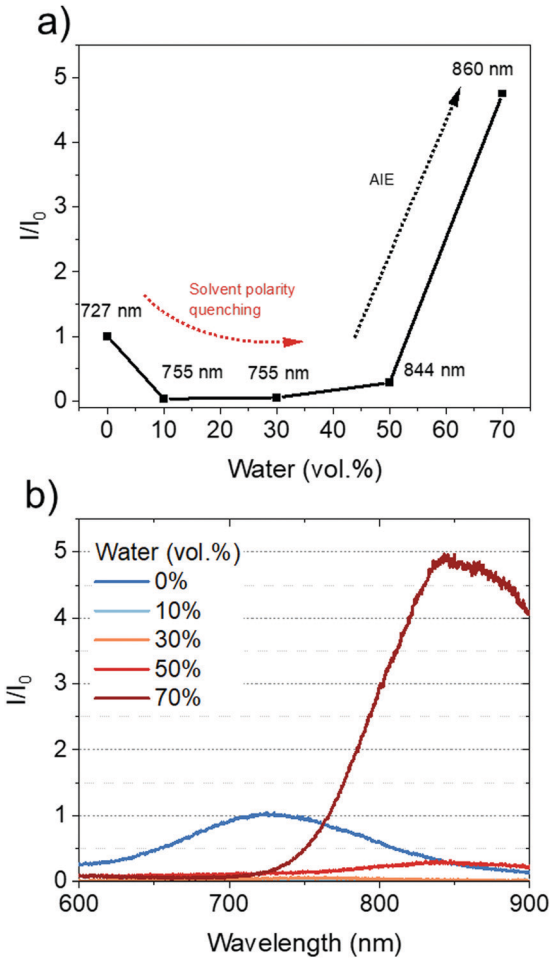

Fig. 4 (a) Intensity normalized PL spectra recorded for CAT-TPE mixtures at different vol% water (λ_{exc} = 400 nm); (b) plot of charge-transfer type photoluminescence intensity *vs.* vol% water in THF for 100 μM **CAT-TPE** mixtures.

We also prepared films of **CAT-1**, for which the TPE groups are absent, doped into TPBi by thermal evaporation (Table S1, ESI†). While a direct quantitative comparison of drop-cast and evaporated samples is tentative due to factors such as differences in film thickness and homogeneity, the PLQYs of **CAT-TPE** films are not significantly depressed compared to those of **CAT-1** at similar PL λ_{max}. In fact, a drop-cast doped film of **CAT-TPE** (5% in TPBi) with PL λ_{max} = 752 nm exhibits Φ_{PL} = 11.3 ± 0.5%, which is higher than for a **CAT-1** film with a similar PL λ_{max} (10% in TPBi, PL λ_{max} = 756 nm, Φ_{PL} = 4.8 ± 0.1%). Such a relationship may be related to the narrower intrinsic bandgap of **CAT-TPE**, which allows *ca.* 750 nm PL at a lower doping concentration that suppresses aggregation-induced quenching (AIQ). Nevertheless, it may appear that the TPE groups of **CAT-TPE** do not have an adverse effect on the quantum efficiency in doped films.

The AIE behavior of **CAT-TPE** was studied in 10^{-4} M THF/water mixtures and the data are shown in Fig. 4. In THF, weak low energy broad PL is observed centered at 727 nm, assigned to CT fluorescence. Upon increasing the water fraction, the CT band red-shifts due to increased solvent polarity and aggregation (Fig. 4a and b). The intensity of the CT band initially drops, before increasing in intensity to a value greater than that of the THF solution, with maximum CT intensity recorded at 70 vol% water. We ascribe this trend to solvent polarity quenching at lower water fractions, which gives way to AIE behavior as the solubility of **CAT-TPE** decreases at higher water fractions (Fig. 4a). This behavior has been commonly reported for ICT AIE emitters.[44–47] To the best of our knowledge **CAT-TPE** is the first example of an all NIR TADF emitter (all CT PL > 700 nm),[48] which is more emissive when aggregated than in solution. This could be promising for biological applications, where the NIR and AIE are both important areas of research.[39,40]

CAT-TPE was next evaluated in solution-processed NIR OLEDs. The data for the reddest device (15 wt% CAT-TPE in TPBi) are shown in Fig. 5 and additional data are included in Fig. S6–S9 and Table S2 (ESI†). The 15 wt% device exhibits no host emission and has EL λ_{max} = 720 nm, exhibiting a maximum EQE of 0.8%. Considering that **CAT-TPE** exhibits TADF and has a PLQY at 10 wt% in TPBi of 2.7 ± 0.1% (Table 2), the max EQE of the 15 wt% device is likely PLQY-limited, presuming good charge balance (~1) and isotropic out-coupling (~0.3). The roll-off performance of the device is also

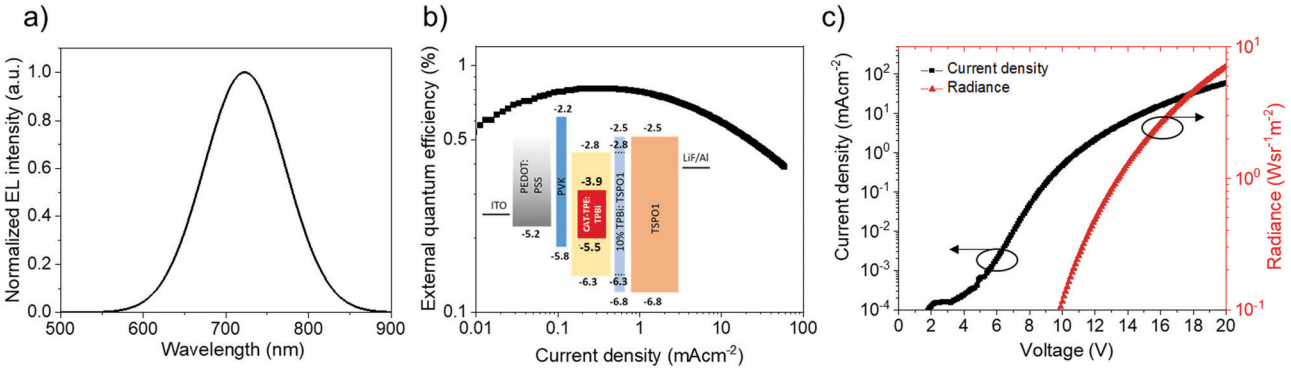

Fig. 5 Electroluminescence characteristics for the 15 wt% **CAT-TPE** device: (a) EL spectrum; (b) plot of EQE *vs.* current density with device structure schematic as inset; (c) plots of current density and radiance *vs.* voltage.

reasonable, dropping to 0.4% EQE at a current density of 50 mA cm^{-2}. For comparison, while a curcuminoid device emitting at an identical EL λ_{max} exhibits a maximum EQE of 9.7%, the roll-off is much more severe, with the EQE decreasing by a factor > 6 to $\sim$1.5% at 50 mA cm^{-2}.[30] We note that the EL of the devices is significantly blue-shifted compared to what would be expected based on PL data. We expect that this can be explained by the variation in preparation technique necessary for PL films *versus* EL OLEDs (*e.g.* solution concentration and temperature, substrate surface and temperature, annealing time). The AIE data reveal the extreme sensitivity of **CAT-TPE** to aggregation-dependent shifting the CT band and it is therefore likely that the solid-state emission is similarly extremely sensitive to the preparation parameters.

Conclusions

Luminophores with fused extended polycyclic electron acceptors constitute the most promising and proven design strategy for efficient NIR TADF. In this work, for the first time, we have extended solution-processability to this class of materials through **CAT-TPE**. TADF was confirmed through variable temperature time resolved measurements at an unprecedented wavelength of 842 nm in a doped film, and an OLED with good roll-off characteristics for solution-processed NIR TADF device was fabricated with EL $\lambda_{max} > 700$ nm.

The solution-processability of **CAT-TPE** was achieved through incorporating tetraphenylethylene (TPE) into the triphenylamine (TPA) donor skeleton. As TPA is the archetypal strong electron donor, ubiquitous in NIR luminophores, our new strategy opens the door to the considerably enhanced structural diversity of solution-processable NIR TADF.

Although **CAT-TPE** retains the common concentration quenching behavior of typical NIR TADF materials, the TPE groups do endow **CAT-TPE** with classic AIE behavior, being more emissive when aggregated than in solution. To the best of our knowledge this is the first report of this property in a NIR TADF material with all CT PL > 700 nm. As well as the promise for biological applications,[41] by pushing AIE TADF truly into the NIR, **CAT-TPE** validates the potential of AIE for reducing non-radiative decay in low bandgap TADF materials.

Author contributions

D. G. C., B. H. D. and Q. G. contributed equally. The manuscript was written through contributions of all authors. D. G. C. and H. B. conceived the research. D. G. C. designed and synthesised the organic materials and contributed to data analysis. B. H. D. performed all solution and solid state photophysical experiments and analysed the data. Q. G. fabricated the OLEDs and analysed the data. S. M. carried out the electrochemical experiments supervised by I. A. W. H. F. and V. R. G. carried out the thermal analysis supervised by C. P. G. W. Z. contributed useful discussion before and during manuscript preparation. C. S. B. M. and S. D. carried out the experiments on evaporated films. R. H. F. supervised B. H. D. and Q. G.

Conflicts of interest

There are no conflicts to declare.

Acknowledgements

D. G. C. acknowledges the Herchel Smith fund for an early career fellowship. This work was supported by the Engineering and Physical Sciences Research Council (grant no. EP/M005143/1) and the European Research Council (ERC). B. H. D. acknowledges support from the EPSRC Cambridge NanoDTC (grant no. EP/L015978/1). Q. G. acknowledges support from Cambridge Trust and China Scholarship Council. S. M. acknowledges Loughborough University for a PhD Studentship. I. A. W. acknowledges the EPSRC (grant no. EP/T028688/1) and RSC (grant no. RF19-2751). V. R. G. and H. F. were supported by the Faraday Institution [grant numbers FIRG001 and FIRG024].

Notes and references

1 G. Qian and Z. Y. Wang, *Chem. – Asian J.*, 2010, **5**, 1006–1029.
2 T. Jiang, Y. Liu, Z. Ren and S. Yan, *Polym. Chem.*, 2020, **11**, 1555–1571.
3 M. Y. Wong and E. Zysman-Colman, *Adv. Mater.*, 2017, **29**, 1605444.
4 M. K. Etherington, *Front. Chem.*, 2020, **8**, 716.
5 F. Ni, N. Li, L. Zhan and C. Yang, *Adv. Opt. Mater.*, 2020, **8**, 1092187.
6 Y. J. Yu, Y. Hu, S. Y. Yang, W. Luo, Y. Yuan, C. C. Peng, J. F. Liu, A. Khan, Z. Q. Jiang and L. S. Liao, *Angew. Chem., Int. Ed.*, 2020, **59**, 21578–21584.
7 J. V. Caspar and T. J. Meyer, *J. Phys. Chem.*, 1983, **87**, 952–957.
8 Y. C. Wei, S. F. Wang, Y. Hu, L. S. Liao, D. G. Chen, K. H. Chang, C. W. Wang, S. H. Liu, W. H. Chan, J. L. Liao, W. Y. Hung, T. H. Wang, P. T. Chen, H. F. Hsu, Y. Chi and P. T. Chou, *Nat. Photonics*, 2020, **14**, 570–577.
9 A. Minotto, I. Bulut, A. G. Rapidis, G. Carnicella, M. Patrini, E. Lunedei, H. L. Anderson and F. Cacialli, *Light: Sci. Appl.*, 2021, **10**, 18.
10 X. Liang, Z. L. Tu and Y. X. Zheng, *Chem. – Eur. J.*, 2019, **25**, 5623–5642.
11 Z. Yang, Z. Mao, Z. Xie, Y. Zhang, S. Liu, J. Zhao, J. Xu, Z. Chi and M. P. Aldred, *Chem. Soc. Rev.*, 2017, **46**, 915–1016.
12 Y. Liu, C. Li, Z. Ren, S. Yan and M. R. Bryce, *Nat. Rev. Mater.*, 2018, **3**, 18020.
13 J. H. Kim, J. H. Yun and J. Y. Lee, *Adv. Opt. Mater.*, 2018, 1800255.
14 Y.-J. Yu, X.-Q. Wang, J.-F. Liu, Z.-Q. Jiang and L.-S. Liao, *iScience*, 2021, **24**, 102123.

15 J.-X. Chen, W.-W. Tao, W.-C. Chen, Y.-F. Xiao, K. Wang, C. Cao, J. Yu, S. Li, F.-X. Geng, C. Adachi, C.-S. Lee and X.-H. Zhang, *Angew. Chem., Int. Ed.*, 2019, **58**, 14660–14665.
16 U. Balijapalli, R. Nagata, N. Yamada, H. Nakanotani, M. Tanaka, A. D'Aléo, V. Placide, M. Mamada, Y. Tsuchiya and C. Adachi, *Angew. Chem., Int. Ed.*, 2021, **60**, 8477–8482.
17 Y. Yuan, Y. Hu, Y. X. Zhang, J. D. Lin, Y. K. Wang, Z. Q. Jiang, L. S. Liao and S. T. Lee, *Adv. Funct. Mater.*, 2017, **27**, 1700986.
18 W. Li, Z. Li, C. Si, M. Y. Wong, K. Jinnai, A. K. Gupta, R. Kabe, C. Adachi, W. Huang, E. Zysman-Colman and I. D. W. Samuel, *Adv. Mater.*, 2020, **32**, 2003911.
19 J. Kumsampao, C. Chaiwai, P. Chasing, T. Chawanpunyawat, S. Namuangruk, T. Sudyoadsuk and V. Promarak, *Chem. – Asian J.*, 2020, **15**, 3029–3036.
20 Q. Liang, J. Xu, J. Xue and J. Qiao, *Chem. Commun.*, 2020, **56**, 8988–8991.
21 K. Zhang, F. Yang, Y. Zhang, Y. Ma, J. Fan, J. Fan, C.-K. Wang and L. Lin, *J. Phys. Chem. Lett.*, 2021, 1893–1903.
22 S. Wang, X. Yan, Z. Cheng, H. Zhang, Y. Liu and Y. Wang, *Angew. Chem., Int. Ed.*, 2015, **54**, 13068–13072.
23 J. Liu, X. Wang, Y. Yu, S. Zou, S. Yang, Z. Jiang and L. Liao, *Org. Electron.*, 2021, **91**, 106088.
24 F. Glöcklhofer, A. J. Morawietz, B. Stöger, M. M. Unterlass and J. Fröhlich, *ACS Omega*, 2017, **2**, 1594–1600.
25 S. Blanc, T. Pigot, C. Cugnet, R. Brown and S. Lacombe, *Phys. Chem. Chem. Phys.*, 2010, **12**, 11280–11290.
26 H. G. Kim, H. H. Choi, E. Song, K. Cho and E. J. Choi, *RSC Adv.*, 2015, **5**, 8070–8076.
27 D. G. Congrave, B. H. Drummond, P. J. Conaghan, H. Francis, S. T. E. Jones, C. P. Grey, N. C. Greenham, D. Credgington and H. Bronstein, *J. Am. Chem. Soc.*, 2019, **141**, 18390–18394.
28 J. Xue, J. Xu, J. Ren, Q. Liang, Q. Ou, R. Wang, Z. Shuai and J. Qiao, *Science China Chemistry*, 2021, **64**, 1786–1795.
29 J. Jin, W. Wang, P. Xue, Q. Yang, H. Jiang, Y. Tao, C. Zheng, G. Xie, W. Huang and R. Chen, *J. Mater. Chem. C*, 2021, 2291–2297.
30 D.-H. Kim, A. D'Aléo, X.-K. Chen, A. D. S. Sandanayaka, D. Yao, L. Zhao, T. Komino, E. Zaborova, G. Canard, Y. Tsuchiya, E. Choi, J. W. Wu, F. Fages, J.-L. Brédas, J.-C. Ribierre and C. Adachi, *Nat. Photonics*, 2018, **12**, 98–104.
31 H. Ye, D. H. Kim, X. Chen, A. D. S. Sandanayaka, J. U. Kim, E. Zaborova, G. Canard, Y. Tsuchiya, E. Y. Choi, J. W. Wu, F. Fages, J.-L. Bredas, A. D'Aléo, J.-C. Ribierre and C. Adachi, *Chem. Mater.*, 2018, **30**, 6702–6710.
32 J. Xue, Q. Liang, R. Wang, J. Hou, W. Li, Q. Peng, Z. Shuai and J. Qiao, *Adv. Mater.*, 2019, 1808242.
33 C. Li, R. Duan, B. Liang, G. Han, S. Wang, K. Ye, Y. Liu, Y. Yi and Y. Wang, *Angew. Chem., Int. Ed.*, 2017, **56**, 11525–11529.
34 J. Mei, N. L. C. Leung, R. T. K. Kwok, J. W. Y. Lam and B. Z. Tang, *Chem. Rev.*, 2015, **115**, 11718–11940.
35 Z. Zhao, H. Zhang, J. W. Y. Lam and B. Z. Tang, *Angew. Chem., Int. Ed.*, 2020, **59**, 9888–9907.
36 Y. Chen, J. W. Y. Lam, R. T. K. Kwok, B. Liu and B. Z. Tang, *Mater. Horiz.*, 2019, **6**, 428–433.
37 S. F. Wang, Y. Yuan, Y. C. Wei, W. H. Chan, L. W. Fu, B. K. Su, I. Y. Chen, K. J. Chou, P. T. Chen, H. F. Hsu, C. L. Ko, W. Y. Hung, C. S. Lee, P. T. Chou and Y. Chi, *Adv. Funct. Mater.*, 2020, **30**, 2002173.
38 Y. Duan, Y. Gao, Q. Pan, Z. Zhao, Y. Wu and L. Zhao, *Dyes Pigm.*, 2021, **194**, 109547.
39 C. Zhu, R. T. K. Kwok, J. W. Y. Lam and B. Z. Tang, *ACS Appl. Bio Mater.*, 2018, **1**, 1768–1786.
40 A. Alabugin, *Photochem. Photobiol.*, 2019, **95**, 722–732.
41 H. Wang, E. Zhao, J. W. Y. Lam and B. Z. Tang, *Mater. Today*, 2015, **18**, 365–377.
42 Y. Liu, X. Chen, Y. Lv, S. Chen, J. W. Y. Lam, F. Mahtab, H. S. Kwok, X. Tao and B. Z. Tang, *Chem. – Eur. J.*, 2012, **18**, 9929–9938.
43 O. Yurchenko, D. Freytag, L. zur Borg, R. Zentel, J. Heinze and S. Ludwigs, *J. Phys. Chem. B*, 2012, **116**, 30–39.
44 G. F. Zhang, M. P. Aldred, W. L. Gong, C. Li and M. Q. Zhu, *Chem. Commun.*, 2012, **48**, 7711–7713.
45 P. Funchien, P. Chasing and V. Promarak, *Chem. Commun.*, 2020, **56**, 6305–6308.
46 W. Yang, C. Li, M. Zhang, W. Zhou, R. Xue, H. Liu and Y. Li, *Phys. Chem. Chem. Phys.*, 2016, **18**, 28052–28060.
47 W. Z. Yuan, Y. Gong, S. Chen, X. Y. Shen, J. W. Y. Lam, P. Lu, Y. Lu, Z. Wang, R. Hu, N. Xie, H. S. Kwok, Y. Zhang, J. Z. Sun and B. Z. Tang, *Chem. Mater.*, 2012, **24**, 1518–1528.
48 A. Zampetti, A. Minotto and F. Cacialli, *Adv. Funct. Mater.*, 2019, **29**, 1807623.

